RESEARCH ARTICLE | DECEMBER 01 2022

Tuning the Čerenkov second harmonic contrast from ferroelectric domain walls via anomalous dispersion

Peter A. Hegarty ⓘ ; Lukas M. Eng ⓘ ; Michael Rüsing ✉ ⓘ

Check for updates

View Online

Export Citation

CrossMark

Tuning the Čerenkov second harmonic contrast from ferroelectric domain walls via anomalous dispersion

Peter A. Hegarty,[1,a)] (ID) Lukas M. Eng,[1,2] (ID) and Michael Rüsing[1,b)] (ID)

AFFILIATIONS

[1]TU Dresden, Institute of Applied Physics, Nöthnitzer Strasse 61, 01187 Dresden, Germany
[2]ct.qmat: Dresden-Würzburg Cluster of Excellence—EXC 2147, TU Dresden, 01062 Dresden, Germany

[a)]Electronic mail: peter_andrew.hegarty@tu-dresden.de
[b)]Author to whom correspondence should be addressed: michael.ruesing@tu-dresden.de

ABSTRACT

Second harmonic (SH) microscopy represents a powerful tool for the investigation of crystalline systems, such as ferroelectrics and their domain walls (DWs). Under the condition of normal dispersion, i.e., the refractive index at the SH wavelength is larger as compared to the refractive index at the fundamental wavelength, $n(2\omega) > n(\omega)$, bulk crystals will generate no SH signal. Should the bulk, however, contain DWs, an appreciable SH signal will still be detectable at the location of DWs stemming from the Čerenkov mechanism. In this work, we demonstrate both how SH signals are generated in bulk media and how the Čerenkov mechanism can be inhibited by using anomalous dispersion, i.e., $n(\omega) > n(2\omega)$. This allows us to quantitatively estimate the relative strength of the Čerenkov compared to other SH contrast mechanisms in DWs, such as the interference contrast. The results are in agreement with previous experiments based on the geometric separation of the signals. Due to the observed, strong Čerenkov contrast, such signal contributions may not be neglected in polarimetry studies of ferroelectric DWs in the future.

I. INTRODUCTION

Second harmonic (SH) microscopy is a flexible imaging and investigation technique into crystalline systems ranging from 2D materials (2DMs) to ferroelectrics and their domain walls (DWs).[1–7] The application of SH microscopy as an imaging process allows for real-time three-dimensional (3D) observation of domain walls (DWs) subjected to external stimuli such as external electric fields[2,5,8] which, combined with no need for special sample preparation, makes it a go-to method for investigations into novel DW structures.[9] Most recently, SH polarimetry has revealed unique symmetries and inherent substructures[6,8,10] previously thought not to be present in ferroelectric DWs and that are believed to be connected to the high conductivity observable in certain DWs.[11,12]

In SH imaging, DWs can appear both as bright lines in a lower signal background, and the other way around, as dark lines in a bright background. As shown many times before, the contrast depends on various conditions, such as the sample orientation, its thickness, or the focusing geometry.[13,14] The contrast for DWs can be explained by three distinct mechanisms that may be present at the same time, making signal interpretation challenging, especially when analyzing the symmetry of DWs.[10] The three broadly accepted mechanisms are:[15]

- (1) interference of the SH signal in the far field from domains of different orientations rather than the DW itself;
- (2) Čerenkov-type phase matching at the DW, termed CSHG; and
- (3) local changes in the nonlinear properties at the DW, which are a central feature in novel symmetries of DWs.[6,10]

In general, contrast mechanisms (1) and (3) can explain both bright and dark DW contrasts depending on the local changes in the SH response,[6,10] as well as the focus placement in relation to the material surface, the light polarization, and the numerical

aperture.[7,13] In contrast, the Čerenkov contrast (2) only results in increased signals stemming from the DWs, i.e., bright DWs.

The Čerenkov SHG effect has been investigated extensively since its first description of this phase-matching scheme in second harmonic generation from thin-film waveguides (optical second harmonic generation in the form of coherent Čerenkov radiation from a thin-film waveguide). In the recent decade, the Čerenkov SHG effect was discovered to be present in ferroelectric DWs and is used as a primary contrast mechanism allowing the visualization of ferroelectric DWs. In this context, various aspects, such as the wavelength dependent emission angle,[15–18] the emission as a function of DW roughness[19] or the existence of collinear CSHG,[3] have been studied. While the DW contrast as a result of (1) interference or (3) local changes in the nonlinear response has been extensively studied in recent years and quantitative models have been developed,[6,7,9,10,13] the strength of CSHG in relation to the other contrast mechanisms is not established, although multiple contrast mechanisms can be present at the same time making separation necessary.[7,15] This is particularly relevant for studies of polarimetry, which mostly rely on interpreting local changes of the SH response. In the present paper, we aim to use the interference contrast as a reference point with which to study the actual contrast and intensity of the Čerenkov effect using the anomalous dispersion regime, which has been shown by Ren *et al.*[20] to block the Čerenkov second harmonic signal. Additionally, this alternative approach will be compared with our previous work,[15] where we applied geometric means to separate the Čerenkov contrast and estimate relative signal strenghts enabling a more complete picture.

The bulk SH Intensity I from a material slab between z_0 and z_1 along the z axis [sketch in Fig. 1(a)] can be calculated in a Gaussian beam picture by

$$I(z_0, \Delta k, b) \propto \left| \int_{z_1}^{z_0} \frac{e^{i\Delta k z'}}{(1 + i2z'/b)} dz' \right|^2. \quad (1)$$

Here, $\Delta k = 2k_\omega - k_{2\omega}$ represents the phase mismatch between the waves at the fundamental (k_ω) and SH frequency ($k_{2\omega}$) [see also Fig. 1(b)], while b is the confocal parameter of the Gaussian beam. Assuming an infinitely thick medium, i.e., setting the boundaries of the integral in Eq. (1) to $\pm\infty$, this integral then converges to two well known results[4,7,21] for either a negative $\Delta k < 0$ or a positive $\Delta k > 0$. For $\Delta k < 0$, this integral yields zero, which is typical for almost all experimental scenarios because the refractive index at the SH wavelength 2ω is *larger* as compared to the refractive index at the fundamental frequency [$n(2\omega) > n(\omega)$]. This condition is also called *normal dispersion* and underlines that SH generation in bulk media using focused beams is not permitted. Under this condition, bulk media only generate signals when the focus is placed close to the surface, i.e., the integration in Eq. (1) is performed only over a semi-infinite range (i.e., from 0 to ∞).

In contrast, for a positive phase mismatch $\Delta k > 0$, the integral will yield a signal even if the focus is placed within the bulk. This so called *anomalous dispersion* is only possible when the refractive index at the SH wavelength is *smaller* than the refractive index at the fundamental wavelength. This can be achieved in birefringent crystals, where an SH process with a switch from one branch of the
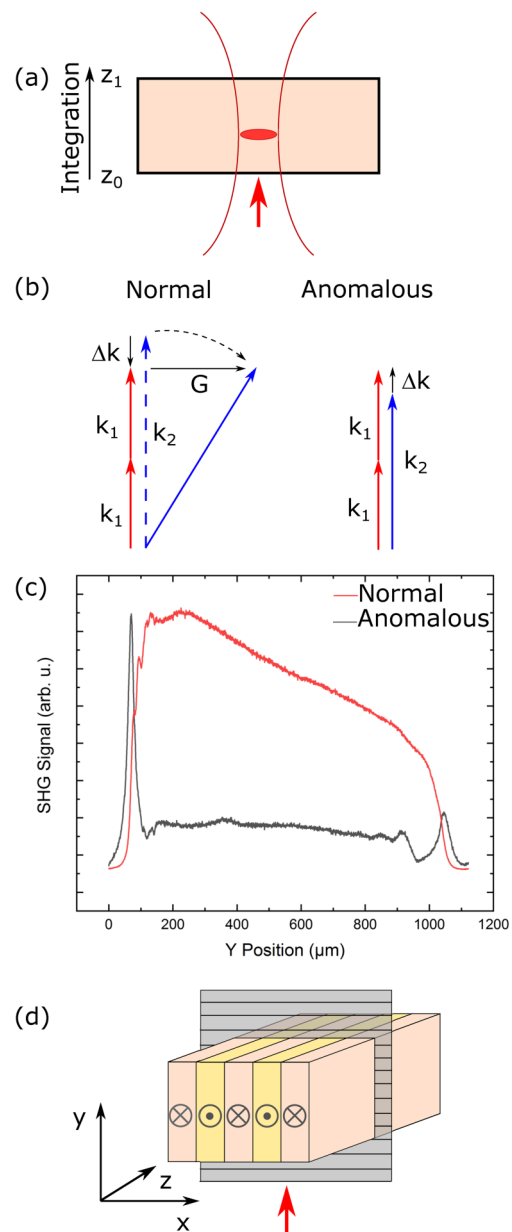

FIG. 1. (a) Sketch of the bulk SH signal calculation according to Eq. (1). (b) Vector diagram comparing the phase-matching process within the normal and anomalous dispersion regime during SH microscopy. (c) shows two experimental scans recorded along the y axis of the crystal, with an incident beam polarized parallel to the x axis using a fundamental wavelength below (black) and above (red) the threshold wavelength for anomalous dispersion. Only the surfaces generate a notable SH signal in normal dispersion, while the entirety of the crystal delivers a signal when operating in the anomalous regime.[4] (d) schematically depicts the investigated periodically poled lithium niobate (PPLN) bars. The laser beam is incident along the crystal's y axis and is polarized along either the x or z axis. A cross section of the xy plane through the crystal is obtained by recording line scans parallel to x in increments of 100 nm along the y axis.

refractive index to the other is possible. In congruent lithium niobate (cLN), for example, this is achieved for a fundamental wavelength beyond 1078 nm via an SH process involving the nonlinear tensor element d_{31}, which allows a fundamental beam in the ordinary polarization (refractive index n_o) to generate signals in the extraordinary polarization (refractive index n_e). For fundamental wavelengths beyond 1078 nm, it holds $n_e < n_o$ fulfilling the condition of anomalous dispersion. Alike, for other dopants in LN, the condition of $n_e < n_o$ may be fulfilled at different wavelengths, as seen from Table I. At the respective threshold wavelength, the refractive indices for both optical directions are equal, i.e., $n_e = n_o$.

Figure 1(c) shows a vertical line scan [red arrow in Fig. 1(d)] through a periodically-poled cLN sample using both normal and anomalous dispersion, that is, the laser beam, polarized parallel to the crystal's x axis, is incident along the crystallographic y axis using a fundamental wavelength above and below 1078 nm, respectively. As previously shown by Kaneshiro et al.,[4] for normal dispersion [black curve in Fig. 1(c)], the surfaces of the crystal generate a SH signal, while the bulk remains relatively dark by comparison. The red curve shows the same location of the sample but with a fundamental wavelength set *above* 1078 nm, where we can see noticeable signal contribution throughout the entire sample, with no pronounced maxima at the surfaces.

As discussed, for normal dispersion, the SH signals in the bulk are zero. Therefore, DWs can only be observed if they have locally different linear or nonlinear properties.[6,24] However, observing DWs in normal dispersion is also possible via the Čerenkov SH process. In a simple picture, the DW acts as an extended defect associated with a lattice momentum Δk that allows for improved (non-collinear) phase matching. As a result, more signal is observed whenever the focus is placed near the DW. This situation is schematically depicted in Fig. 1(b) through the respective wave vector matching. The Čerenkov SHG is generally generated at an oblique angle compared to the fundamental beam, although collinear CSHG has also been reported.[3] This, however, requires further analysis of additional DW properties such as the inclination angle and roughness, we will, therefore, focus on the non-collinear case and the influence of anomalous dispersion on the DW contrast as a whole. The oblique emission is only possible for normal dispersion, as $k_{2\omega}$ needs to be larger than $2k_\omega$. Therefore, choosing an SH process under the conditions of anomalous dispersion will also prohibit the generation of Čerenkov SH generation. For imaging of

TABLE I. Threshold wavelengths for the anomalous regime for different types of lithium niobate (LN), these being stoichiometric LN (sLN), (5%) magnesium-oxide-doped LN (MgO:LN) and undoped congruent LN (cLN). The theoretical threshold wavelengths, where it holds $n_e = n_o$, were calculated using the Sellmeier formulas published by Edwards et al. (a temperature-dependent dispersion equation for congruently grown lithium niobate), Zelmon et al.,[22] and Jundt et al.[23] for congruent, magnesium-doped, and stoichiometric LN, respectively. At wavelengths larger than this threshold and for processes involving the d_{31} tensor elements, the conditions for anomalous dispersion are fulfilled.

Material	sLN	MgO:LN	cLN
Theoretical threshold (nm)	980	1034	1078
Experiment (nm)	…	1060 ± 10	1090 ± 10

DWs in bulk crystals, this has important consequences. As Čerenkov is forbidden in this case, any changes of the DW signal can only be attributed to either interference effects or changes in the local nonlinear susceptibility, which now can be studied systematically.

In this work, we show that the choice of the fundamental wavelength allows us to selectively turn on or off the Čerenkov mechanism by switching from normal ($\Delta k < 0$) to anomalous dispersion ($\Delta k > 0$) for a fixed focal position at a DW within the crystal. While in the past, experiments either well below or well above this threshold have been performed,[4,20] in this work, we particularly focus on the transition region. This enables us not only to change the contrast from bright to dark, but also to get a quantitative insight into the Čerenkov contrast mechanism as well, which has eluded quantitative predictions of the contrast so far, and compare it with the much better understood interference contrast. The experimental work performed here can serve as a reference for quantitative analysis of the CSHG contrast, in a similar manner as the interference contrast has been analyzed.

II. EXPERIMENTAL SETUP

The investigated samples were bars cut from a z-cut wafer of both periodically-poled congruent (cLN) and (5%) magnesium-oxide-doped lithium niobate (MgO:LN). The bars are then rotated 90° onto their y face. This allows access to both the ordinary refractive index (n_o) using a beam polarized parallel to the crystallographic x axis as well as to the extraordinary refractive index (n_e) with a beam polarized parallel to the z axis. The utilized setup is a Zeiss LSM980MP microscope operated in transmission, equipped with a linearly-polarized, tunable Ti:Sa laser (Spectra Physics InSight X3, 690–1300 nm, 3,5 W, <120 fs pulse width) for excitation, using a focusing NA of 0.8 and collection NA of 0.55 in the forward direction.

Figure 1(d) depicts a sketch of the measurement geometry including a visualization of the xy plane scanned through the sample. The DWs investigated in this work lay within the zy plane of the sample, and our scans will, therefore, depict them as continuous vertical lines in the images.

III. RESULTS AND DISCUSSION

To display whether or not the proposed switching in contrast is observed, images were recorded for the cLN sample at 1050 and 1100 nm fundamental wavelengths, i.e., above and below the theoretical threshold wavelength. Two scattering geometries are chosen:

- (1) The fundamental laser is polarized parallel to the x-direction of the crystal (n_o). Here, the SH signal will be dominantly generated via the bulk d_{31} tensor element and be polarized in z-direction (n_e). In this geometry, a switch from normal to anomalous dispersion is expected.
- (2) In the second geometry, the fundamental laser is polarized parallel to the z axis (n_e). Here, SH light is generated via the largest tensor element d_{33} and is also polarized along the z-direction of the crystal. Hence, no effect is expected.

The results of these four experiments are depicted in Fig. 2. Figures 2(a) and 2(b) depict the first scattering geometry for 1050

and 1100 nm, respectively, while Figs. 2(c) and 2(d) show the second scattering geometry without a switch to anomalous dispersion. The dashed white lines in Figs. 2(a) and 2(b) represent the location from which the signal profile was extracted at a depth of $500\,\mu m$ within the crystal for later analysis, as then displayed in Fig. 3. During measurements using geometry (1), a small amount of ordinarily polarized SHG light will also be generated via the d_{22} element. However, due to the smaller magnitude of this tensor element as well as its shorter coherent interaction length, the process via the d_{31} will largely dominate, as has been shown previously.[14,15]

As mentioned above, for normal dispersion, we expect the DWs to appear as bright lines on a dark background due to the $20\times$ stronger signal generation from the Čerenkov mechanism combined with the lack of bulk signal.[15] On the other hand, for the anomalous dispersion regime, we expect a negative contrast between DW and domains, i.e., the DWs are dark lines, as well as a noticeable signal from the domains themselves.

Below the threshold wavelength, both geometries qualitatively display the same behavior, i.e., the domain walls are visible as bright lines on the dark background of the bulk material. However, the signal obtained from the second geometry is noticeably larger likely due to the incident polarization being parallel to the largest non-linear tensor element d_{33} in lithium niobate. Please note, while
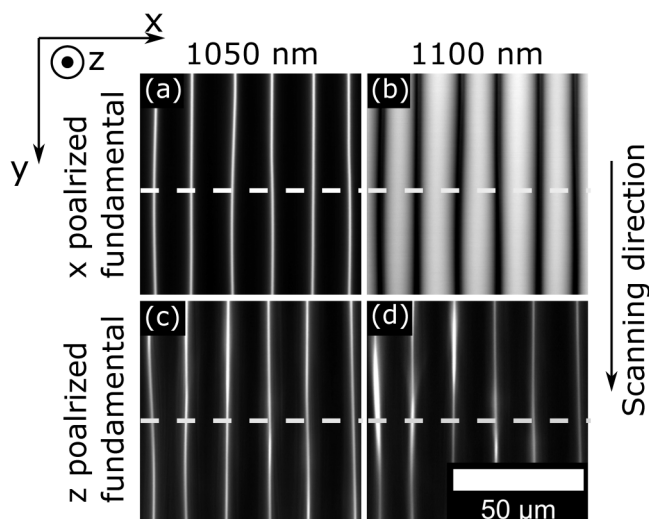
FIG. 2. Comparison images of the SH signal generated within the bulk of a periodically-poled congruent lithium niobate crystal. (a) and (b) are images recorded with an x polarized fundamental beam. We see a difference in generated signal, as for the anomalous regime, the bulk domain is the majority source of the signal, while the domain walls appear dark compared to the bright DWs on a dark background as in (a). (c) and (d) show the case of a z polarized fundamental beam. Here, the images remain the same regardless of fundamental wavelength and consist of bright lines on a dark background, analogously to (a). The slight variations in the DW signal is most likely an indication of small meanderings or kinks within the domain wall, rather than a result of the chosen incident wavelength, as the DWs do not develop uniformly during the poling process.
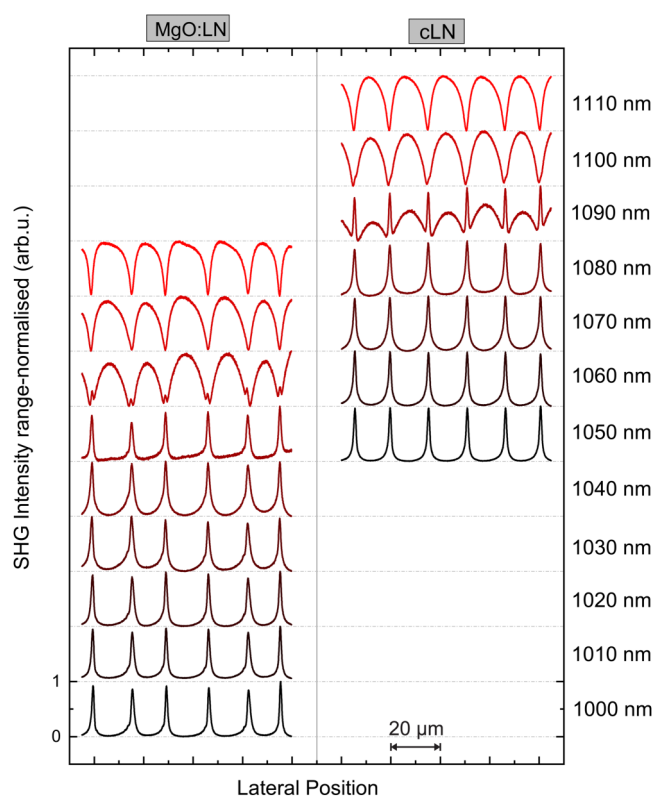
FIG. 3. Lateral scans extracted as cross sections from images such as those shown in Fig. 2 for a range of different wavelengths between 1000 and 1110 nm plotted for both periodically poled MgO:LN (left) and cLN (right). Each profile is normalized to the [0,1] intensity scale to allow for a closer comparison of their behavior. We observe a positive DW signal below each crystal's threshold (black colored profile), i.e., the DW is brighter than the surrounding domain, e.g., for MgO:LN at 1000 nm, whereas the DW appears as a drop in signal in the anomalous regime and the domains themselves deliver signal (red colored profile), e.g., 1080 nm for MgO:LN. The change between the two types of profiles appears to be gradual, close to the expected threshold wavelengths, we observe a superposition of the two contrast types, e.g., at 1060 nm for MgO:LN.

the same crystal was analyzed, the region that is visualized is different, as the crystal needed to be physically rotated due to the fixed polarization of the laser in the setup (to maintain the exact same illumination conditions, the sample is rotated by 90° rather than the incident laser polarization).

The difference between both geometries becomes apparent for the images recorded at 1100 nm. Here, the second geometry recreates a similar image, while for the first geometry, however, we see that the domain walls appear as dark lines on a white background, i.e., the CSHG light previously generated at the lower wavelength is suddenly no longer part of the emitted signal, while the bulk material generates significant SH signal in agreement with theory.[4] Additionally, the measurable signal generated by the domain regions opens the door toward analysis performed on the bulk domains themselves, rather than an analysis limited to the domain

walls within the bulk. Further images recorded at intermediate wavelengths in the present cLN crystal as well as cross sections for periodically-poled MgO:LN are included in Figs. S1 and S2 in the supplementary material.

So far, the analysis was limited to single wavelengths above or below the threshold. However, for an in-depth analysis of the competing mechanisms, the behavior in the vicinity of the threshold wavelength requires investigation. We calculated the theoretical threshold wavelengths as the wavelength for which $n_o(\omega) = n_e(2\omega)$, which are listed in Table I.

Measurements similar to Figs. 2(a) and 2(b) were then recreated using a range of wavelengths for periodically-poled cLN and MgLN crystals around the calculated threshold in y steps of 10 nm. As we are interested in the bulk behavior neglecting any influence of surface effects, signal profiles were extracted at a depth of $500\,\mu m$ within the crystal, as indicated by the dashed lines in Figs. 2(a) and 2(b).

Due to the stark difference in the overall signal between the experiments at different fundamental wavelengths, for example, due to the largely different coherent interaction lengths, each profile was normalized to achieve comparability. For this work, we chose two types of normalization. First, each profile was normalized to the interval [0,1]. This was specifically used in Figs. 2 and 3 as well as Figs. S1 and S2 in the supplementary material. This normalization particularly highlights the nature of the line shapes and qualitative behavior of the contrast. Second, the data were normalized to the bulk intensity, which directly highlights the contrast as defined below. Here, after dark count subtraction, where necessary, the intensity was normalized to the intensity value measured in the bulk in between two domain walls, which consequently has an intensity of unity. This type of normalization was also used on previous works, where the DW contrast was analyzed numerically.[7,9] The respective data can be found in Figs. S3 and S4 in the supplementary material for cLN and MgO:LN, respectively.

The resulting data are plotted in Fig. 3, with data recorded at the same fundamental wavelength displayed at the same height in the image. As with the images in Fig. 2, on the high or low end of the recorded wavelength ranges, the DWs appear solely as a positive or negative peak, respectively. More clearly, for MgO:LN, DWs at a 1000 nm wavelength give a positive SH response (black), whereas they appear "negative" at 1080 nm (red). In fact, as the wavelength in each material closes in on the threshold wavelength, we observe a decreasing contrast between DW and the neighboring domain signal, although the profile is still dominated by a single positive or negative peak.

At approximately the calculated threshold wavelength, a flip in contrast is observed. However, this flip is not sudden, but continuous over a range of >30 nm in wavelength, which is due to the spectral width of the exciting ultra short laser pulse ($FWHM \approx 15$ nm at 1000 nm). A range of wavelengths makes up the incident pulse, of which a certain fraction may still be below the threshold. The result should be a superposition of the two peak types. This can be seen for 1060 nm in the case of MgO:LN and 1090 nm in the case of cLN, where a central peak belonging to the Čerenkov contrast emerges from the dip belonging to the interference contrast dominating in the anomalous dispersion region. Interestingly, in both materials, we observe this superposition at a

larger wavelength than expected theoretically for monochromatic incident light.

The determined thresholds are summarized in Table I. Here, we observe that the measured thresholds are off from the expected wavelength in both materials by approximately +26 nm (MgO:LN) and +12 nm (sLN), respectively. In contrast, the relative order in threshold wavelength is reproduced, i.e., threshold wavelength in sLN is larger compared to MgO:LN). Here, likely reasons are deviations from ideal conditions, e.g., temperature, as well as stoichiometric variations in the different compositions of LN, which is known to have an impact on the dispersion. Indeed, in previous work, we also observed slight systematic shifts of thin-film resonances compared to theoretical calculations, which likely also indicated variations of stoichiometry or conditions.[14]

Previous work has shown that the Čerenkov SHG responsible for the bright domain walls within the bulk is approximately 20 times stronger than the other contrast mechanisms in SH microscopy.[15] As a result, it would require less incident light below the anomalous threshold to generate a signal comparable to "traditional" SHG from the surrounding domain, which is caused by the wavelengths above the threshold. This would explain the apparently higher threshold wavelength, as the vast majority of the spectral components of the pulse would have to be far beyond the actual threshold. For further analyis of the influence of anomalous dispersion, the DW signal contrast was calculated. Within this work here, we define the contrast C as the quotient of the difference in signal magnitude between DW (S_{DW}) and domain (S_{Domain}), and the average domain signal, i.e.,

$$C = \frac{S_{DW} - S_{Domain}}{S_{Domain}} = \frac{S_{DW}}{S_{Domain}} - 1. \quad (2)$$

The sign of the contrast C now indicates the type of DW contrast, as a negative contrast value infers that the DWs are darker than the average domain signal and vice versa for a positive contrast. Additionally, the absolute magnitude gives an indication of the strength thereof. Figure 4(a) depicts the extraction of the contrast as shown in Eq. (2).

Figures 4(b) and 4(c) display the DW contrast as a function of depth and wavelength for the example of the CLN sample. For each parameter setting, the DW contrast values were averaged across the DW signatures in profiles such as those shown in Fig. 3.

In Fig. 4(b), the contrast is plotted as a function of depth for 1050, 1090, and 1110 nm, i.e., at wavelengths below, approximately at, and above the anomalous dispersion threshold, respectively. The contrast values for 1050 nm were scaled down to a factor of 0.05 to allow for comparison within the same range. Here, the contrast at the outermost wavelengths is dominated by a single type of contrast throughout the sample thickness, negative above the threshold with $C \approx -0.6$, and $C \approx 16$ below the threshold, while close to the threshold, an overlapping of both mechanisms is present.

For the wavelength well above the threshold, it is interesting to note that the contrast value for 1110 nm is centered around $C \approx -0.6$, i.e., the DW signal is 0.4 times the domain signal. In simulations of SH microscopy of ferroelectric domain walls, Rüsing *et al.* showed that the expected ratio between DW and domain signal is approximately -0.6 in thin films inspected in reflection
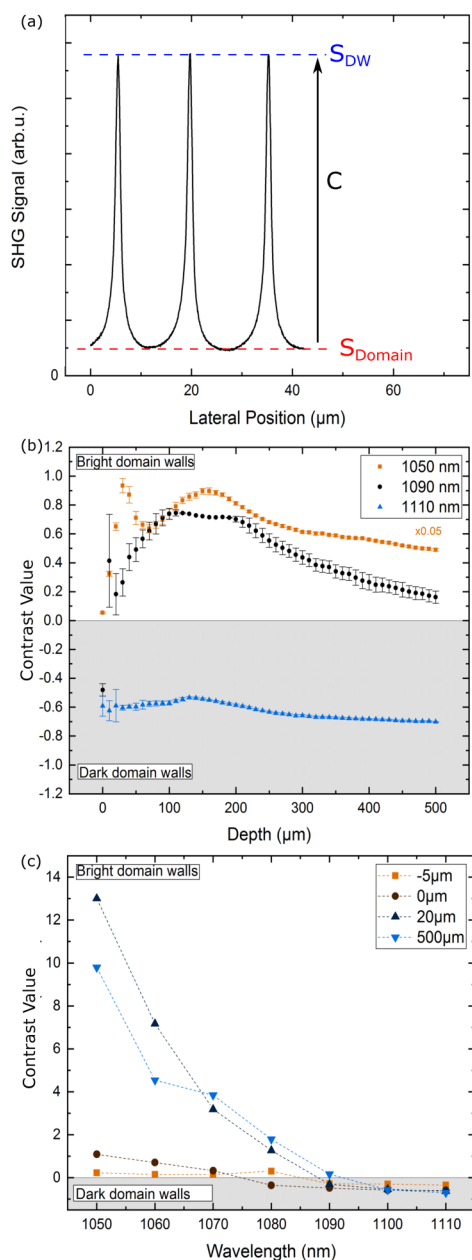
FIG. 4. (a) Visualization sketch to clarify the definition of contrast in this work, the extracted value is then put into relation to the average bulk signal to calculate the contrast value. (b) Contrast values for three different wavelengths plotted as a function of depth into the crystal. Both 1050 and 1110 nm are well within their respective regime and show the characteristic behavior thereof, while the values calculated for 1090 nm display a slight superposition of both. (c) Contrast values at four different locations within the crystal plotted vs the fundamental wavelength. Within the normal regime, we observe fully positive contrast whereas for the anomalous regime the contrast is entirely negative. Within the transition region, the type of contrast begins to vary with depth, as we observe a negative contrast at the surface (0 μm), whereas the contrast remains positive for all other locations at a fundamental wavelength of 1080 nm.

geometry, and is a result of phase interference between overlapping SH waves from neighboring domains.[9] The positive contrast for Čerenkov SHG of $C \approx 16$ is comparable to our previous experiments with blocking apertures.[15] The error bars in Fig. 4(b) were calculated from the standard deviation of the contrast value. Generally, we see a low error within both regimes (orange and blue), while the transition region can show a slightly higher variance due to the competing mechanisms and low contrast in itself.

When examined closer, the lines approximately at (1090 nm) and below the threshold (1050 nm) show a general decrease in contrast, in particular, for a larger depth. This behavior resembles the overall decrease in intensity with depth as shown in Fig. 1(c) and likely relates to the decrease in focus power density due to the temporal broadening of the pulse and spatial broadening of the focal spot in larger depth. This observation provides a hint, that the temporal shape and/or focus spot shape also influences the CSHG contrast. For a fundamental wavelength of 1050 nm close to the threshold a negative contrast is observed close to the surface, which then flips to a slightly positive $C \approx 0.6$ at increasing depth. The negative contrast close to the surface can be explained by strong interference type contrast, which dominates due to the strong SHG from interfaces also in the case of normal dispersion.[4,7] It is similarly observed for a fundamental wavelength of 1050 nm, where the contrast first shows a low value of $C \approx 1$ close to the surface due to overlapping of interference contrast. For increasing depth at this fundamental wavelength, the contrast rapidly grows to a value of almost 20 at depth of 30 μm. However, the contrast stays not constant but shows another local minimum in a depth of about 70 μm with $C \approx 12$. As can be seen in Fig. S5 in the supplementary material, such a minimum is also present for 1060 nm and almost disappears for larger wavelengths. The origin of this local minimum is not clear. One potential explanation for this effect could be an influence of axial phase matching, which explains the slight shift to larger depth for increasing wavelengths and the disappearance close to the threshold wavelength, where the coherent interaction length converges to infinity. Similar minima were also observed in previous work.[4] However, in contrast to Kaneshiro *et al.,* in our case, only negligible bulk SHG signal for a fundamental wavelength of 1050 and 1060 nm is observed. Therefore, this minimum is only present in the Cerenkov signal. For further insight, more theoretical work is indicated.

Figure 4(c) shows the average contrast as a scatterplot vs fundamental wavelength for four selected depths, these being shortly (-5μm) before the surface, exactly at the surface (0 μm), at an intermediate depth (20 μm), and far within the bulk (500 μm). Generally, we see that the average DW contrast decreases with increasing wavelength, eventually showing a fully negative contrast for 1100 nm and above, regardless of the extraction depth. When comparing the chosen depths over the entire wavelength range, it is possible to group them into a surface-near and surface-far behavior. The monotonous decrease of the contrast, instead of a step-like switching at the threshold wavelength may be explained by the spectral width of the pulse, which has an FWHM of approximately 15 nm at 1000 nm, as discussed for Fig. 3 as well. This means that certain parts of the pulse are already at or beyond the threshold, which will result in a contrast below 1 due to the interference contrast, which will decrease in the overall contrast. The highest values

of $C \approx 13$ in Fig. 4(c) at the lowest wavelength and a depth of $500\,\mu m$ are of similar order as observed at even lower wavelength in our previous experiment.[15] It can be expected that for lower wavelengths, a constant contrast of the order of $C \approx 15 - 20$ will be observed.

Shortly before the surface ($-5\,\mu m$), the contrast is close to 0, because there is only a low signal generation, as only a fraction of the focus is placed within the sample. The comparably low contrast directly at the surface ($0\,\mu m$) can also be explained by the strong surface-SHG signal, which is generated regardless of which dispersion regime the experiment is performed in. Independent of the fundamental wavelength, simulations predict a negative contrast for the surface in the investigated geometry due to a strong contribution from interference contrast,[7,9] which in this experiment appears to be overlapped by a positive contrast from the Čerenkov effect. Despite the lower contrast magnitude, however, the contrast for both depths is positive far within the normal regime, i.e., at 1050 nm, and negative only far within the anomalous regime, i.e., at 1110 nm. This could indicate a lower energy density requirement at the DWs for generating CSHG.

The contrast values extracted at depths of 20 and $500\,\mu m$ show a strong positive value of up to 13 and 10, respectively, for wavelengths below the threshold. The contrast rapidly decreases with increasing fundamental wavelength before transitioning to a negative contrast at 1090 nm and higher. The notably large contrast within the normal dispersion regime is caused by the CSHG signal generated at the DWs as well as the absence of bulk signals from the domain regions. As seen in the blue data points of Fig. 4(b), in the anomalous regime, the contrast settles into a value of approximately $C \approx -0.6$ regardless of depth, which is a result of the absence of CSHG. Here, the contrast can only be attributed to interference or local changes in non-linearity.

IV. CONCLUSION

In conclusion, we have investigated the influence of the dispersion on contrast in SH microscopy of ferroelectric DWs. It is shown that, in continuation of Kaneshiro *et al.*,[4] above a certain threshold wavelength, it is possible to generate SH signal from the bulk rather than the DWs of a periodically-poled lithium niobate crystal. Far from the aforementioned threshold, we observe a signal dominated by either CSHG or another SH mechanism, such as interference contrast, respectively. Examining the contrast close to the threshold, it becomes obvious that multiple processes are present at the same time. However, if SH generation from bulk is forbidden, the strong CSHG signal[15] overpowers the other contributions. This potentially has implications for the study of DW substructures via SHG polarimetry, which is gaining recent interest in bulk and thin films alike.[6,10]

The choice of wavelength and process is shown to be a valid parameter when performing SH microscopy to selectively disable CSHG, granting access to the signal stemming from phase interference and changes to the local non-linearity without the dominating contribution of CSHG. Additionally, the generation of SH signals within bulk domains allows for analyzing the domain regions themselves rather than being limited to the DWs, e.g., the addition of a known reference crystal could allow for the determination of

the local polarization orientation via interference imaging.[4] For example, from studies with Raman spectroscopy of ferroelectric DWs, it is known that long range strain fields exist, which extend at least several micrometers around the domain transition.[25] This may explain the large FWHM of the domain transitions observed in Fig. 3 in the anomalous regime but requires further studies.

Ideally, this investigation into anomalous dispersion in SH microscopy can serve as a novel approach in separating the participating contrast mechanisms and developing a more advanced understanding of ferroelectric materials and their DWs.

SUPPLEMENTARY MATERIAL

See the supplementary material for a full compilation of the cross-section images shown in Fig. 2 for both cLN and MgO:LN as well as further plots of the extracted signal profiles which retain the relative peak magnitudes between wavelengths for both crystals.

AUTHOR DECLARATIONS

Conflict of Interest

The authors have no conflicts to disclose.

Author Contributions

Peter A. Hegarty: Data curation (equal); Formal analysis (equal); Investigation (equal); Methodology (equal); Writing – original draft (equal); Writing – review & editing (equal). **Lukas M. Eng:** Funding acquisition (equal); Methodology (equal); Supervision (equal); Writing – original draft (equal); Writing – review & editing (equal). **Michael Rüsing:** Funding acquisition (equal); Methodology (equal); Supervision (equal); Writing – original draft (equal); Writing – review & editing (equal).

DATA AVAILABILITY

The data that support the findings of this study are available from the corresponding author upon reasonable request.

REFERENCES

[1]W. Murray, M. C. Lucking, E. Kahn, T. Zhang, K. Fujisawa, N. Perea-Lopez, A. L. Elias, H. Terrones, M. Mauricio Terrones, and Z. Liu, "Second harmonic generation in two-dimensional transition metal dichalcogenides with growth and post-synthesis defects," 2D Mater. 7, 045020 (2020).
[2]T. Kämpfe, P. Reichenbach, M. Schröder, A. Haußmann, L. M. Eng, T. Woike, and E. Soergel, "Optical three-dimensional profiling of charged domain walls in

ferroelectrics by Cherenkov second-harmonic generation," Phys. Rev. B **89**, 035314 (2014).

[3]T. Kämpfe, P. Reichenbach, A. Haußmann, T. Woike, E. Soergel, and L. Eng, "Real-time three-dimensional profiling of ferroelectric domain walls," Appl. Phys. Lett. **107**, 152905 (2015).

[4]J. Kaneshiro, S. Kawado, H. Yokota, Y. Uesu, and T. Fukui, "Three-dimensional observations of polar domain structures using a confocal second-harmonic generation interference microscope," J. Appl. Phys. **104**, 054112 (2008).

[5]B. Kirbus, C. Godau, L. Wehmeier, H. Beccard, E. Beyreuther, A. Haußmann, and L. Eng, "Real-time 3D imaging of nanoscale ferroelectric domain wall dynamics in lithium niobate single crystals under electric stimuli: Implications for domain-wall-based nanoelectronic devices," ACS Appl. Nano Mater. **2**, 5787 (2019).

[6]S. Cherifi-Hertel, H. Bulou, R. Hertel, G. Taupier, K. Dorkenoo, C. Andreas, J. Guyonnet, I. Gaponenko, K. Gallo, and P. Paruch, "Non-Ising and chiral ferroelectric domain walls revealed by nonlinear optical microscopy," Nat. Comm. **8**, 15768 (2017).

[7]K. Spychala, P. Mackwitz, A. Widhalm, G. Berth, and A. Zrenner, "Spatially resolved light field analysis of the second-harmonic signal of $\chi^{(2)}$-materials in the tight focusing regime," J. Appl. Phys. **127**, 023103 (2020).

[8]U. Acevedo-Salas, B. Croes, Y. Zhang, O. Cregut, K. D. Dorkenoo, B. Kirbus, E. Singh, H. Beccard, M. Rüsing, L. M. Eng, R. Hertel, E. A. Eliseev, A. N. Morozovska, and S. Cherifi-Hertel, "Impact of 3D curvature on the polarization orientation in non-Ising domain walls," 2207.01307 [cond-mat.mtrl-sci] (2022).

[9]M. Ruesing, J. Zhao, and S. Mookherjea, "Second harmonic microscopy of poled x-cut thin film lithium niobate: Understanding the contrast mechanism," J. Appl. Phys. **126**, 777 (2019).

[10]S. Cherifi-Hertel, C. Voulot, U. Acevedo-Salas, Y. Zhang, O. Crégut, K. Dorkenoo, and R. Hertel, "Shedding light on non-Ising polar domain walls: Insight from second harmonic generation microscopy and polarimetry analysis," J. Appl. Phys. **129**, 081101 (2021).

[11]C. Godau, T. Kämpfe, A. Thiessen, L. Eng, and A. Haußmann, "Enhancing the domain wall conductivity in lithium niobate single crystals," ACS Nano **11**, 4816 (2017).

[12]H. Beccard, B. Kirbus, E. Beyreuther, M. Rüsing, P. Bednyakov, J. Hlinka, and L. M. Eng, "Nanoscale conductive sheets in ferroelectric BaTiO$_3$: Large Hall electron mobilities at head-to-head domain walls," ACS Appl. Nano Mater. **5**, 8717 (2022).

[13]K. Spychala, P. Mackwitz, M. Rüsing, A. Widhalm, G. Berth, C. Silberhorn, and A. Zrenner, "Nonlinear focal mapping of ferroelectric domain walls in LiNbO$_3$: Analysis of the SHG microscopy contrast mechanism," J. Appl. Phys. **128**, 234102 (2020).

[14]Z. Amber, B. Kirbus, L. Eng, and M. Rüsing, "Quantifying the coherent interaction length of second-harmonic microscopy in lithium niobate confined nanostructures," J. Appl. Phys. **130**, 133102 (2021).

[15]P. A. Hegarty, H. Beccard, L. M. Eng, and M. Rüsing, "Turn all the lights off: Bright- and dark-field second-harmonic microscopy to select contrast mechanisms for ferroelectric domain walls," J. Appl. Phys. **131**, 244102 (2022).

[16]A. Fragemann, V. Pasiskevicius, and F. Laurell, "Second-order nonlinearities in the domain walls of periodically poled KTiOPO$_4$," Appl. Phys. Lett. **85**, 375–377 (2004).

[17]Y. Sheng, A. Best, H.-J. Butt, W. Krolikowski, A. Arie, and K. Koynov, "Three-dimensional ferroelectric domain visualization by Čerenkov-type second harmonic generation," Opt. Express **18**, 16539–16545 (2010).

[18]Y. Sheng, S. Saltiel, N. Voloch-Bloch, D. Neshev, W. Krolikowski, A. Arie, K. Koynov, and Y. Kivshar, "Cerenkov-type second-harmonic generation in two-dimensional nonlinear photonic structures," J. Quantum Electr. **45**, 1465 (2009).

[19]X. Deng and X. Chen, "Domain wall characterization in ferroelectrics by using localized nonlinearities," Opt. Express **18**, 15597 (2010).

[20]H. Ren, X. Deng, Y. Zheng, N. An, and X. Chen, "Nonlinear Cherenkov radiation in an anomalous dispersive medium," Phys. Rev. Lett. **108**, 223901 (2012).

[21]J. Kaneshiro, Y. Uesu, and T. Fukui, "Visibility of inverted domain structures using the second harmonic generation microscope: Comparison of interference and non-interference cases," J. Opt. Soc. Amer. B **27**, 888 (2010).

[22]D. Zelmon, D. Small, and D. Jundt, "Infrared corrected Sellmeier coefficients for congruently grown lithium niobate and 5 mol. % magnesium oxide-doped lithium niobate," J. Opt. Soc. Am. B **14**, 331 (1997).

[23]D. Jundt, M. Fejer, and R. Byer, "Optical properties of lithium-rich lithium niobate fabricated by vapor transport equilibration," IEEE J. Quantum Electron. **26**, 135 (1990).

[24]J. Golde, M. Rüsing, J. Rix, L. M. Eng, and E. Koch, "Quantifying the refractive index of ferroelectric domain walls in periodically poled LiNbO$_3$ single crystals by polarization-sensitive optical coherence tomography," Opt. Express **29**, 33615 (2021).

[25]M. Rüsing, S. Neufeld, J. Brockmeier, C. Eigner, P. Mackwitz, K. Spychala, C. Silberhorn, W. G. Schmidt, G. Berth, A. Zrenner, and S. Sanna, "Imaging of 180° ferroelectric domain walls in uniaxial ferroelectrics by confocal Raman spectroscopy: Unraveling the contrast mechanism," Phys. Rev. Mater. **2**, 103801 (2018).